

## Research Paper

# Spectroscopic follow-up of the quadruply lensed quasar WGD2038-4008/GRAL2038-4008

Chien-Hsiu Lee

National Optical Astronomy Observatory, 950 N Cherry Ave., Tucson, AZ 85719, USA

### Abstract

We present independent optical spectroscopic follow-up of WGD2038-4008/GRAL2038-4008, a background quasar strongly lensed by a foreground elliptical galaxy into four images, recently discovered independently by Agnello et al. [2018, MNRAS, 479, 4345] and Krone-Martins et al. [2018, A&A, 616, L11] thanks to the exquisite spatial resolution of Gaia. The quasar images are bright ( $i \sim 19$  mag), thus enabling us to reach  $S/N > 20$  for the continuum within 30 min of exposure time with the Andalucia Faint Object Spectrograph and Camera spectrograph mounted on the 2.56-m Nordic Optical Telescope. The flexible scheduling and high sensitivity delivered by Andalucia Faint Object Spectrograph and Camera provide timely redshifts and reveal the nature of the quasar images; both are essential for lensing modelling and cosmography. Our analysis shows a strong emission feature in a data gap in Agnello et al. [2018, MNRAS, 479, 4345], which can be attributed to as an interloper emission line feature from the foreground lensing galaxy, or hinting to a higher redshift of the background quasar. We discuss these two scenarios and outline possible tests to verify these scenarios.

**Keywords:** catalogues – gravitational lensing: strong – quasars: general – surveys – techniques: image processing

(Received 27 October 2018; revised 12 December 2018; accepted 22 January 2019)

### 1. Introduction

In the era of precision cosmology, determining and comparing the Hubble constant ( $H_0$ ) down to 1% level both locally and at high redshifts can provide leverages on the nature of dark energy, physics of neutrinos, and the curvature of Universe. On the local side, using the distance ladder, the SH0ES team has dramatically reduced the  $H_0$  error budget to 2.3% (Riess et al. 2018) and showed tension (at  $3.4\sigma$  level) with the Planck CMB results at higher redshift. Though tempting to claim such tension may lead to signs of new physics, it is important to investigate both systematics in the Planck measurement and to have independent local  $H_0$  measurement than SH0ES.

An ideal alternative is gravitational lensing time-delays. The working principle is that for a background source that is strongly lensed and split into multiply images from observer's perspective, the photons from each image will undergo different light path before reaching the observer. Since the difference of light travel time (or time-delay) only depends on the space-time curvature, we can therefore infer  $H_0$  accordingly. In this regard, quadruply lensed quasars are especially useful than doubly lensed ones, because they can provide a factor of two more time-delay information. The state-of-the-art  $H_0$  estimate from gravitational lensing time-delay comes from the HOLiCOW team (Suyu et al. 2017). So far HOLiCOW used three quadruply lensed quasars (each has  $H_0$  estimate to 7–8%) and determined  $H_0$  to 3.8% level (Bonvin et al. 2017). While there was a recent claim by Tie & Kochanek

(2018) that microlensing effects might bring additional significant effects on the uncertainty of time-delay measurements (hence impacts the  $H_0$  estimate), it has been shown from Chen et al. (2018) that microlensing only affects short time-delays ( $<20$  d) and has insignificant effect on longer time-delays (with tens of days).

While tens of quadruply lensed quasars are known to exist, with Hubble Space Telescope (HST) data,<sup>a</sup> only few of them are suitable to estimate  $H_0$ , with known quasar and lens redshifts and measurable variability. In order to use gravitational lensing time-delay for cosmography, we need detailed modelling of the lensing system, which relies upon accurate spectroscopic redshifts of the background quasar. In this paper, we aim to refine the redshift measurements of a newly discovered quadruply lensed quasar candidate WGD2038-4008 from Dark Energy Survey (DES), and independently from Gaia DR2 (GRAL2038-4008) by Krone-Martins et al. (2018). The bright quasar images have the advantages of enabling high S/N photometry even with small-to-medium-class telescopes, which will allow us to determine the time-delay in a short (several months) monitoring fashion (Courbin et al. 2017).

This paper is organised as follows. In Section 2, we present independent spectroscopic observations and the redshift estimates from these newly acquired spectra, featuring a strong emission feature that was in the data gap of Agnello et al. (2018). In Section 3, we discuss possible origins of this feature, including an interloper from the foreground lensing galaxy, or a higher redshift of the background quasar. We also provide other means that can verify our redshift estimate, via either high-resolution spectrum of the lens or time-series photometry of the quasar. Our findings are summarised in Section 4.

**Author for correspondence:** Chien-Hsiu Lee, Email: [lee@noao.edu](mailto:lee@noao.edu)

**Cite this article:** Lee Chien-Hsiu. (2019) Spectroscopic follow-up of the quadruply lensed quasar WGD2038-4008/GRAL2038-4008. *Publications of the Astronomical Society of Australia* 36, e011, 1–4. <https://doi.org/10.1017/pasa.2019.4>

© Astronomical Society of Australia 2019; published by Cambridge University Press.

<sup>a</sup>For example, <https://www.cfa.harvard.edu/castles/>.

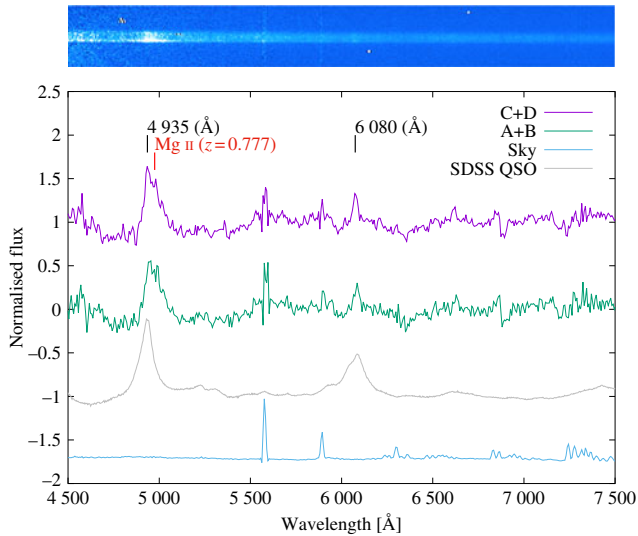


**Figure 1.** Follow-up spectra of WGD2038-4008 from ALFOSC. Upper panel: 2D spectra of image A+B. Although the spectra were taken under mediocre seeing condition, we can still see the trace of image A (upper part) and image B (lower part) in the spectra. There are two apparent emission features at observed wavelength of  $\sim 4935$  and  $\sim 6080$  Å, respectively. In the 2D spectra we can also see residuals of sky lines from sky subtraction at  $\sim 5600$  and  $5800$  Å. Lower panel: 1D spectra of image A+B (green) and image C+D (purple). We normalised the spectra according to the flux of the continuum. In addition, we also show SDSS composite quasar spectrum from vanden Berk et al. (2001) redshifted to  $z = 2.187$  for comparison (in grey), as well as the sky spectrum (in blue colour, flux not to scale) to aid identifying false emission features in the 1D extracted spectra.

## 2. Long-slit spectrograph observation

As the four images of the background quasar are rather bright ( $i \sim 19$  mag), medium telescopes are sufficient to reach reasonable spectral S/N in a modest amount of time. To derive the spectroscopic redshifts of the background quasar in a timely manner, we obtain optical spectra of WGD2038-4008 taking advantages of the fast-track service programme of the Andalucia Faint Object Spectrograph and Camera (ALFOSC) mounted on the 2.56-m Nordic Optical Telescope (NOT) at La Palma Observatory on the Canary Island. The observations were carried out on 2018 June 9 with median seeing of 1.2 arcsec. We observed WGD2038-4008 using Grism No. 4 with a  $2 \times 2$  binning through a 1.0-arcsec width slit. We employed two positional angles of  $33^\circ$  and  $-50^\circ$ , going through image pair C&D and A&B, respectively. For each slit position, we dither the long-slit in an A-B-B-A pattern, with a dithering step of 1 arcsec to allow us to remove bad pixels and cosmic rays. The individual exposure time at each dithering position is 450 s. In the end we acquired a total on-source time of 30 min at each slit orientation. In addition, we also took images of bias and flat fields, as well as spectra of Th-Ar lamp for wavelength calibration.

Data reduction was carried out in a standard manner using the Image Reduction and Analysis Facility (IRAF)<sup>b</sup>. Each 2D spectrum was bias subtracted, flat fielded, wavelength calibrated against the Th-Ar lamp spectra, and then sky subtracted. We then median-combined the 2D spectra to better remove cosmic rays and bad pixels. We then extracted the 1D spectra and normalised them by fitting the continuum with 10th-order polynomials. The 2D spectra, as well as the extracted, normalised 1D spectra, are shown in Figure 1.

<sup>b</sup><http://iraf.noao.edu>.

We note that, however, due to the mediocre seeing condition and the large pixel scale from  $2 \times 2$  binning, we cannot clearly separate and extract spectrum from each quasar image. Nevertheless we were able to extract the spectrum of image pairs, that is, quasar image A+B, and image C+D, into 1D spectra. From the 2D spectra, we can clearly see two emission lines at  $\sim 4935$  and  $\sim 6080$  Å, where the later one is in the data gap of Agnello et al. (2018). In the following section, we discuss two scenarios that can corroborate the presence of both emission features at  $\sim 4935$  and  $\sim 6080$  Å, that is, (1) the 6080 Å is an interloper emission line from the foreground lensing galaxy and (2) both the 4935 and 6080 Å features belong to the background source, hinting at a higher redshift of the background quasar.

## 3. Discussion

Given the lens redshift of  $z_l = 0.23$  (Agnello et al. 2018), the  $\sim 6080$  Å emission line feature is at about the right redshift of [O III] 5007. In fact, if we use the  $H\gamma$  absorption line, we will obtain a slightly lower redshift of  $z_l \sim 0.22$ , which is within the error to have [O III] 5007 at  $\sim 6080$  Å. However, we should note that [O III] emission line is a signature of star-forming galaxies, but the high-resolution HST images and lens modelling (Shajib et al. 2018) both indicate that the foreground lensing galaxy is an elliptical galaxy, hard to reconcile with strong [O III] 5007 emission.

On the other hand, both the  $\sim 4935$  and  $\sim 6080$  Å emission line features can also originate from the background source. To explore this possibility, we first use the broad-band photometry to have a initial guess of the photometric redshift.

The optical photometry of WGD2038-4008 has been measured by Agnello et al. (2018). In addition, we also analyse the near-infrared images obtained by the VISTA Hemisphere Survey (VHS)<sup>c</sup> using the 4-m VISTA telescope in Chile. The images were taken under seeing condition of  $\sim 0.7$  in both  $J$  and  $K_s$  bands. We download the photometric calibrated and astrometrically aligned infrared images from the VISTA science archive (VSA) at the Royal Observatory, Edinburgh,<sup>d</sup> for further analysis. Our analysis is based on the data release 5 version of the VHS. As the four quasar images and the foreground lens are blended in the VHS images, we use the GALFIT package (Peng et al. 2002, 2010) to extract the photometry of each component. The four quasar images are modelled with a point-spread function (PSF) constructed from  $\sim 20$  bright stars within  $5 \times 5$  arcmin. We also model the foreground lens using a Sersic profile. This results in an effective radius of  $R_e \sim 2.3$  arcsec in  $J$  and 1.7 arcsec in  $K_s$ , and a Sersic index of 3.4 in  $J$  and 2.0 in  $K_s$ , respectively. The best-fit GALFIT models are shown in Figure 2; the photometry of each quasar image is shown in Table 1.

With the optical and infrared photometry in hand, we then proceed to estimate the photometric redshift. We correct for the line-of-sight extinction using the values from Schlafly & Finkbeiner (2011). We assume  $R_v = 3.1$  and use the extinction law of Cardelli, Clayton, & Mathis (1989) to calculate the un-extincted magnitudes in each pass-bands. We then compared the de-reddened photometry to a quasar spectrum, convolved with the filter responses to the Dark energy survey camera filters<sup>e</sup> and the VISTA near-infrared filters<sup>f</sup>, using the Photometric Analysis for Redshift Estimate

<sup>c</sup><http://www.vista-vhs.org>.

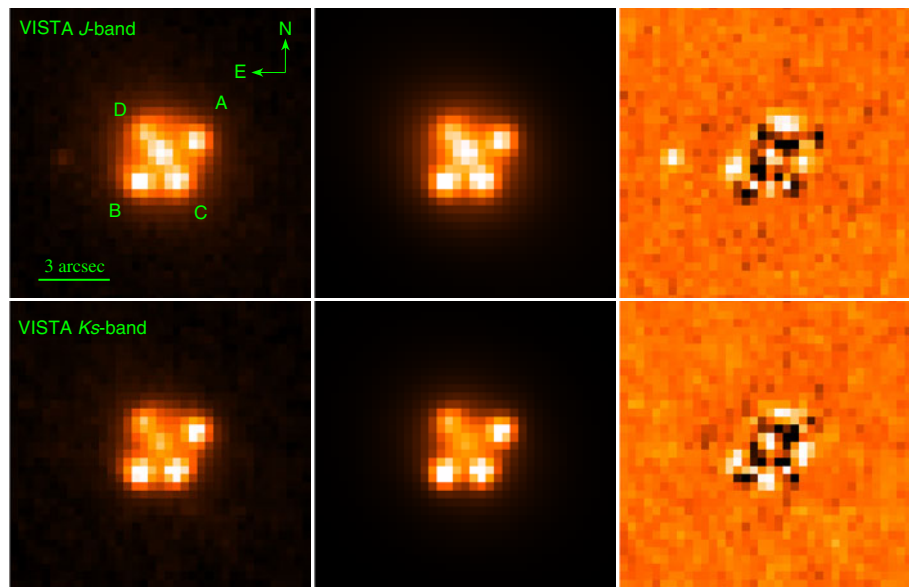
<sup>d</sup><http://horus.roe.ac.uk/vsa/>.

<sup>e</sup><http://www.ctio.noao.edu/noao/content/DECam-filter-information>.

<sup>f</sup><https://www.eso.org/sci/facilities/paranal/instruments/vircam/inst.html>.

**Table 1.** Optical and infrared photometry of WGD2038-4008. The listed values are AB magnitudes.

ID	<i>g</i>	<i>r</i>	<i>i</i>	<i>z</i>	<i>Y</i>	<i>J</i>	<i>Ks</i>
A	20.22 ± 0.03	19.74 ± 0.03	19.24 ± 0.03	18.67 ± 0.03	18.96 ± 0.03	16.75 ± 0.03	15.01 ± 0.03
B	20.08 ± 0.04	19.45 ± 0.04	18.98 ± 0.04	18.50 ± 0.05	18.71 ± 0.03	16.47 ± 0.03	14.80 ± 0.03
C	20.17 ± 0.04	19.50 ± 0.04	19.08 ± 0.03	18.58 ± 0.03	18.66 ± 0.03	16.56 ± 0.03	14.84 ± 0.03
D	20.99 ± 0.05	19.91 ± 0.06	19.42 ± 0.06	19.95 ± 0.05	19.24 ± 0.10	16.485 ± 0.05	15.07 ± 0.05

**Figure 2.** Left column: VISTA images of WGD2038-4008. Middle column: Best-fit models of the four quasar images (using PSF) and the foreground lens (using Sersic profile) from GALFIT. Right column: Residuals of the observed images minus that of the best-fit model. We note that the residuals exhibit a ring-like shape, suggesting features from the extended quasar host galaxy as seen from Shajib et al. (2018). The upper and lower rows are *J* and *Ks* bands, respectively.

package<sup>8</sup> (LePhare, Arnouts et al. 1999; Ilbert et al. 2006). LePhare estimates photometric redshifts between 2.4 and 2.8 for all four quasar images. This suggests that the quasar has a redshift higher than 2. Assuming a higher  $z_s$ , we found that the  $\sim 4935$  and  $\sim 6080$  Å emission line features correspond to a redshift of  $z \sim 2.2$  for C IV line at 1549 Å and C III line at 1909 Å, respectively. From the 1D spectra in Section 2, we fit a Gaussian function to the redshifted C IV and C III emission lines to determine their centroid and infer the redshift to be  $z = 2.187 \pm 0.004$ .

This scenario suggests that the background quasar is at a higher redshift of 2.187, significantly differs from the spectroscopic redshift in the literature. We note that it is difficult to understand the true causes that lead to the large difference between the spectroscopic redshift of  $z = 2.187$  derived from our analysis and the value of  $z = 0.777$  reported by Agnello et al. (2018). This is especially the case as Agnello et al. (2018) do not provide details of their spectroscopic observations, reduction and analysis (e.g., which emission lines are used to derive the redshift). On top of that, we do not have access to the raw data of Agnello et al. (2018). Hence we can only speculate that the most likely cause is the spectra of Agnello et al. (2018) are contaminated by the sky lines at the red end of the spectrum, and these sky lines at the red end of the spectrum are confused with quasar emission lines when determining the redshifts. This is the case when checking their Figure 4 for

the 1D spectra of WGD2038-4008; the most prominent emission lines are at observed wavelength of  $\sim 8600$ ,  $8800$ , and  $8900$  Å that can be regarded as H $\beta$  and the [O III] doublet at a putative redshift of  $z = 0.777$ . However, there are numerous sky lines in this wavelength range and might be confused as quasar emission lines if the sky subtraction is not perfect. In addition, in their Figure 4 there is an emission feature at observed wavelength of  $4900$  Å, which will be stronger than the emission features at  $8600$ – $8900$  Å if we normalised the 1D spectrum, and this emission feature cannot be reconciled with the putative  $z = 0.777$ . This is especially the case because the putative Mg II at  $z = 0.777$  is off the peak of the broad emission feature at  $4900$  Å, as can be seen in Figure 4 of Agnello et al. (2018) and in Figure 1 of this work. Besides, the emission features at  $8600$ – $8900$  Å are also present in the 1D spectrum of another lens WGD2021-4115 (albeit weak), hence hinting at imperfect sky subtraction. In addition, there is an emission line at  $\sim 6600$  Å, presumably the [O II] 3727 assuming  $z = 0.777$  from Agnello et al. (2018). However, this feature only appears in the spectrum of B+C, but not in G+D. It is the same for another emission line feature at  $\sim 5900$  Å. Both the  $5900$  and  $6600$  Å emission lines are sharp and narrow and only present in the spectrum of B+C but not in G+D, hinting to possible imperfect cosmic-ray removal.

Besides these speculation, we can also verify/test whether  $z = 2.187$  is the correct spectroscopic redshift with other approaches. First of all, given the Einstein ring radius  $\theta_E$  (which can be robustly determined from lens modelling of the image) and the redshifts

<sup>8</sup><http://www.cfht.hawaii.edu/~arnouts/lephare.html>.

of the lens and the background source, we can calculate the lens velocity dispersion  $\sigma_v$  as follows (see, e.g., Narayan & Bartelmann 1996):

$$\sigma_v \sim 10^3 \frac{\text{km}}{\text{s}} \sqrt{\frac{\theta_E}{28''} \frac{D_s}{D_{ds}}}, \quad (1)$$

where  $D_s$  is the distance to the background source and  $D_{ds}$  is the distance between the source and the lens (deflector).

A putative  $z=0.777$  will result in a  $\sigma_v$  of 303 km/s, while  $z=2.187$  will lead to a  $\sigma_v$  of 289 km/s assuming a  $\Lambda$  cosmology with  $h_0$  of 0.7 and  $\Omega_M = 0.3$ . In this regard, high-resolution spectra of the lens will help measure  $\sigma_v$  and thus verify the redshift of the background quasar.

Another possibility is to use time-delays from different quasar images to verify the redshift of the background quasar. The time-delay can be expressed as (Narayan & Bartelmann 1996)


$$t(\vec{\theta}) = \frac{1+z_d}{c} \frac{D_d D_s}{D_{ds}} \left[ \frac{1}{2} (\vec{\theta} - \vec{\beta})^2 - \Psi(\vec{\theta}) \right], \quad (2)$$

where  $\Psi(\vec{\theta})$  is the lensing potential,  $\vec{\theta}$  and  $\vec{\beta}$  are the angular separations of the lensed image and the background source from the optical axis as viewed by the observer, respectively. Using  $z_s=0.777$ , Shajib et al. (2018) predict  $\Delta t_{AB} = -6$  d,  $\Delta t_{AC} = -11$  d, and  $\Delta t_{AD} = -27$  d, respectively. If the background quasar were at  $z=2.187$  instead, the time-delays will be  $-5.5$ ,  $-10.0$ , and  $-24.6$  d, respectively. We note that the time-delays are only  $\sim 10\%$  difference between  $z=0.777$  and  $z=2.187$ , which would require a very accurate time-delay measurements. On the other hand, this implies that the quasar would not be useful for measuring  $H_0$  through time-delays if the redshift was not established.

#### 4. Summary

We present independent optical spectroscopic follow-up of WGD2038-4008, covering the data gap of Agnello et al. (2018). In addition, we also carry out infrared modelling and photometry

of WGD2038-4008 from archival VHS images. The infrared photometry, along with the optical photometry from the literature, predicts a photometric redshift of  $z > 2$ . Our spectral analysis also suggests that the background quasar is at redshift of  $z=2.187$  from the C IV and C III emission lines. The difference between our redshift estimate and that from the literature might stem from imperfect sky line removal. We outline possible tests that can verify the higher redshift scenario using lens velocity dispersion or time-delays. Further high-resolution spectra of the lens, or high-cadence photometric monitoring of the quasar images are highly encouraged.

**Author ORCIDs.**  Chien-Hsiu Lee <https://orcid.org/0000-0003-1700-5740>

**Acknowledgements.** We are indebted to the anonymous referee, whose comments greatly improved this manuscript. This article is based on observations made in the Observatorio de Canarias del IAC with the NOT operated on the island of La Palma by the Nordic Optical Telescope Scientific Association. The data presented here were obtained with ALFOSC, which is provided by the Instituto de Astrofísica de Andalucía (IAA) under a joint agreement with the University of Copenhagen and NOTSA.

#### References

- Agnello, A., et al. 2018, MNRAS, 479, 4345  
 Arnouts, S., et al. 1999, MNRAS, 310, 540  
 Bonvin, V., et al. 2017, MNRAS, 465, 4914  
 Cardelli, J. A., Clayton, G. C., & Mathis, J. S. 1989, ApJ, 345, 245  
 Chen, G. C.-F., et al. 2018, MNRAS, 481, 1115  
 Ilbert, O., et al. 2006, A&A, 457, 841  
 Krone-Martins, A., et al. 2018, A&A, 616, L11  
 Narayan, R., & Bartelmann, M. 1996, [arxiv.9606001](https://arxiv.org/abs/9606001)  
 Peng, C. Y., Ho, L. C., Impey, C. D., & Rix, H.-W. 2002, AJ, 124, 266  
 Peng, C. Y., Ho, L. C., Impey, C. D., & Rix, H.-W. 2010, AJ, 139, 2097  
 Riess, A. G., et al. 2018, ApJ, 855, 136  
 Schlafly, E. F., & Finkbeiner, D. P. 2011, ApJ, 737, 103  
 Shajib, A. J., et al. 2018, MNRAS, 483, 5649  
 Suyu, S. H., et al. 2017, MNRAS, 468, 2590  
 Vanden Berk, D. E., et al. 2001, AJ, 122, 549  
 Tie, S. S., & Kochanek, C. S. 2018, MNRAS, 473, 80